Modeling and control of crystal shape in continuous protein crystallization

Joseph Sang-Il Kwon [a], Michael Nayhouse [a], Panagiotis D. Christofides [a,b], Gerassimos Orkoulas [a,*]

[a] Department of Chemical and Biomolecular Engineering, University of California, Los Angeles, CA 90095, USA
[b] Department of Electrical Engineering, University of California, Los Angeles, CA 90095, USA

HIGHLIGHTS

- Kinetic Monte Carlo simulation of protein crystal growth.
- Approximate model for evolution of protein crystal shape in continuous crystallization.
- Model predictive control of protein crystal shape in a continuous crystallizer.
- Disturbance handling using model predictive control.

ARTICLE INFO

ABSTRACT

In this work, a continuous crystallization process with a fines trap is modeled in an effort to produce tetragonal hen-egg-white (HEW) lysozyme crystals with a desired shape distribution. The crystal shape of tetragonal lysozyme crystals is defined by the aspect ratio of the crystal heights in the direction of the (110) and (101) faces. A kinetic Monte Carlo (kMC) simulation is used to model the crystal nucleation, growth, and dissolution through a fines trap in a continuous crystallization process. Specifically, the crystal growth processes are simulated through adsorption, desorption, and migration mechanisms, and the crystal growth rates are calibrated through experimental data (Durbin and Feher, 1986). Additionally, a nucleation rate expression is developed based on the results from an experimental work (Galkin and Vekilov, 2001) to simulate the crystals nucleated at different times. Then, the method of moments is used to approximate the dominant behavior of a population balance equation (PBE) describing the evolution of the crystal volume distribution through the three leading moments. The moment model is used, along with solute mass and energy balance equations, to design a model predictive controller (MPC), which allows for the crystallizer to produce crystals with a desired shape distribution. In the proposed MPC, the jacket temperature is manipulated to appropriately suppress the influence of undesired effects such as process disturbances and measurement noise, while handling significant changes in the set-point value. Furthermore, it is demonstrated that a continuous process with a fines trap can produce crystals with a low polydispersity.

© 2013 Elsevier Ltd. All rights reserved.

1. Introduction

Protein crystallization is essential in the context of separation and purification processes in the pharmaceutical industry. More than 90% of all active pharmaceutical ingredients (API) are in the crystalline form of organic compounds. Depending on the final dosage form (e.g., tablet, capsule, liquids, syrups, creams and injections), the production of API crystals with desired size and shape distributions is required for bioavailability and stability of the final dosage forms, because size and shape distributions significantly influence the physical properties of the crystalline APIs (e.g., dissolution rates in the blood and melting points). In particular, when the products are off the desired specification, additional downstream processes (e.g., filtration, drying, and granulation) are needed. Therefore, the modeling of the crystallization process in an effort to control the size and shape distributions of crystals produced from the system is necessary to facilitate the further development of pharmaceutical processes.

Over the last few decades, batch processes have received dominant attention in the pharmaceutical industry. In batch

* Corresponding author. Tel.: +1 310 267 0169; fax: +1 310 206 4107.
E-mail address: makis@seas.ucla.edu (G. Orkoulas).

operations, a drug's APIs are synthesized and then carried to other facilities where they are turned into a large amount of a desired final dosage form. Although the research and development period plays a major role in the time-to-market, the inefficiency owing to the distant nature of facilities involved in the crystallization processes will cause additional delay in the time-to-market and it will be handled through a series of continuous crystallizers. Additionally, due to the nature of a batch process, there are a number of issues that need to be addressed such as batch-to-batch variability, high equipment and operational costs, and relatively long separation time of the APIs (Lawton et al., 2009).

Recently, continuous crystallization, which is able to consistently produce crystals with desired size and shape distributions starting from fresh raw materials, is receiving growing attention in the pharmaceutical industry. Specifically, once a steady-state has been achieved in a continuous crystallizer, all crystals are produced under a uniform supersaturation level, which leads to greater reproducibility and controllability of major characteristics of crystals such as size and shape distributions. As a result, the number of downstream operations required to amend crystals with undesired size and shape distributions (e.g., granulation for the solid dosage forms) may be reduced.

Consequently, using a continuous manufacturing process can stimulate the growth of the pharmaceutical industry as it may reduce the size of production facilities, operating costs, waste, energy consumption, and raw material usage considerably. Moreover, the reproducibility and controllability of the APIs in the final dosage form can be improved.

Motivated by above, researchers have made notable advancements in the context of fundamental understanding and modeling of protein crystallization for crystal nucleation (Galkin and Vekilov, 1999; Pusey and Nadarajah, 2002) and crystal growth (Durbin and Feher, 1986; Forsythe et al., 1999; Kurihara et al., 1996). Specifically, kinetic Monte Carlo simulation methods (kMC) (Bortz et al., 1975; Dai et al., 2005, 2008; Gillespie, 1976, 1977, 1978, 1992, 2001, 2007; Rathinam et al., 2003; Reese et al., 2001; Snyder et al., 2005) have been widely applied to simulate crystal growth including the previous work of our group (Nayhouse et al., 2013, Kwon et al., 2013a, 2013b, in press) where we modeled crystal growth in batch processes. In the present work, the kMC methodology is further developed to model a continuous protein crystallization process, and implemented in the way described in Christofides et al. (2008) using the rate equations on the crystal surface reaction initially developed by Durbin and Feher (1991).

Then, a population balance model for a continuous crystallization process with a fines trap is presented. In practice, the complexity in a population balance model usually leads to an implementation issue with the controller design (Chiu and Christofides, 1999). Therefore, the method of moments is used to derive reduced-order ordinary differential equation (ODE) models in time, which are used to approximate the dominant behavior of the evolution of crystal volume distribution in a continuous crystallizer (El-Farra et al., 2001; Kalani and Christofides, 2002). In order to close the moment model, a normal distribution assumption is used to approximate the crystal volume distribution. In addition to a set of polynomials that describes the dependence of crystal growth of each face on a supersaturation level, the mass and energy balance equations and the moment models are considered to design a model predictive control (MPC) system, which is used to produce crystals with a desired shape distribution. To improve the controller performance, an advanced real-time monitoring technique is necessary in practice, because the damage is irreversible if the produced crystals are off the desired specification at the outlet of the process. Motivated by this, the measurements of crystals through the use of focused beam reflectance measurement (FBRM) and process vision and
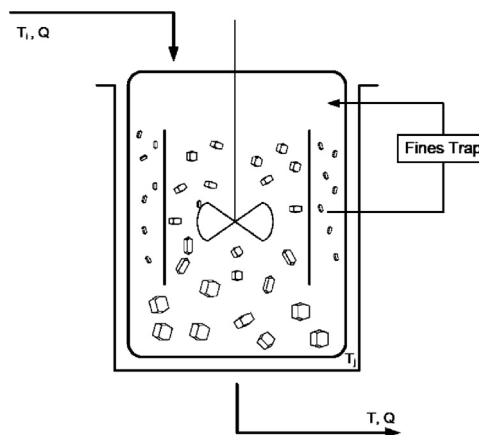

Fig. 1. MSMPR crystallizer used in this work.

measurement (PVM) (Kougoulos et al., 2005) are modeled as measurement system feedback in real time from the kMC simulations, which is treated as the physical crystallization process.

The manuscript is organized as follows. First, we will introduce a continuous crystallization process with a fines trap. Then, the crystallizer rate equations used for the implementation of the kMC simulation method will be introduced. Next, a set of mass and energy balances will be presented along with a PBM of the crystal volume distribution, and the method of moment will be used to construct a reduced-order model for the design of a model predictive controller, which will drive the shape distribution of crystal population to a desired value. Finally, we will finish with closed-loop simulation results under the proposed MPC, followed by a short conclusion.

2. Process descriptions

2.1. Continuous crystallizers

There are two types of the most widely used continuous crystallizers in the pharmaceutical industry: mixed suspension mixed product removal (MSMPR) and plug flow reactors (PFR). The choice of which to use is mainly determined by the characteristics of the process, as MSMPR is generally preferred for low conversions and longer residence times, while PFR is preferred for higher conversions with shorter residence times. In general, MSMPR is preferred because it is relatively similar to the conventional batch process (Chen et al., 2011).

The low conversion in MSMPR can be improved by strategies such as the addition of a recycle stream or the addition of a fines trap. More specifically, an increase in yield was observed by Alvarez et al. (2011) and Wong et al. (2012) through the implementation of recycle streams to MSMPR systems for the crystallization of cyclosporine. Additionally, it was demonstrated that the multistage MSMPR approach was simplified into a single-stage MSMPR by implementing a recycle stream and a fines trap (Griffin et al., 2010).

A fines trap is one of the most widely used product classification processes, and it can be established, first of all, by shielding a part of a mixed crystallizer with a baffle as is shown in Fig. 1. As a result, the circulation of the continuous phase through the baffled region is typically slow, and larger crystals sink to the bottom of crystallizer while small crystal fines float on the top where a stream is drawn off and sent to the fines trap where small crystals are dissolved and are recycled back to the crystallizer. By manipulating the stirrer speed in the baffled continuous crystallizer, we can control the maximum particle size L_{max} that will enter the

fines trap stream. Specifically, while we can easily control the flow rate Q of a stream to the crystallizer, it is rather difficult to model and control the motion of particles which is under the influence of shear forces induced by agitation. In this work, we assumed that the extent of aggregation is negligible because the residence time of a continuous process is typically 1 or 2 h, and thus the average crystal size of the final products is not large enough to get influenced by the shear force due to stirring significantly. Furthermore, a fines trap can considerably reduce the number of crystals, and thus it lowers the collision rates between crystals.

3. Description and modeling of continuous crystallization process

3.1. Crystal nucleation

In this work, only primary nucleation of HEW lysozyme is considered. Motivated by Nanev and Tsekova (2000), Suzuki et al. (1994) and Kwon et al. (2013b), we assumed that crystals are nucleated with infinitesimal size (i.e., $V=0$). The subsequent fate of the nucleus whether to grow or dissolve into the continuous phase is determined by the amount of the free energy required for the formation of the crystal structure versus the free energy required for the formation of the surface adjacent to the continuous phase. We defined the supersaturation $\sigma = \ln(C/s)$ as the difference in chemical potential between the current state, C (mg/mL), and the saturated state, s (mg/mL). The nucleation rate at pH=4.5 and 4%(w/v) NaCl, $B(\sigma)$, is obtained from Galkin and Vekilov (2001):

$$B(\sigma) = \begin{cases} 0.041\sigma + 0.063 & \text{for } \sigma \geq 3.11 \\ 8.0 \times 10^{-8} \exp(4.725\sigma) & \text{for } \sigma < 3.11 \end{cases} \tag{1}$$

with units (cm^{-3} s^{-1}). Also, the solubility is an explicit function of temperature T ($^{\circ}$C) and is computed using the following expression (Cacioppo et al., 1991; Cacioppo and Pusey, 1991):

$$s(T) = 2.88 \times 10^{-4} T^3 - 1.65 \times 10^{-3} T^2 + 4.62 \times 10^{-2} T + 6.01 \times 10^{-1}. \tag{2}$$

3.2. Modeling of crystal growth and dissolution

In most crystallization processes, the solute molecules move from the bulk solution to the crystal surface and then they are converted into the crystalline form through surface reaction. The diffusion coefficient is usually high in crystallization systems, and thus the crystal growth is primarily controlled by the surface reaction (reaction-limited). As a result, the growth rate becomes size-independent, and it is usually assumed that the dissolution rate is also size-independent because the dissolution process is the reverse of the growth process (Majumder and Nagy, 2013).

For the purpose of comparison, the crystal is assumed to be equidimensional. As is given by Schmidt (2005), the time necessary to grow a lysozyme crystal from $R_0=1$ to $R=10$ μm, assuming that the growth is reaction-limited, can be calculated as follows:

$$t_{rxn} = \frac{\rho_B}{k'' C_A M_B}(R - R_0)$$

Similarly, the time necessary to grow a lysozyme crystal from R_0 to R, assuming that the growth is mass-transfer-limited, is

$$t_{mt} = \frac{\rho_B}{2 D_A M_B C_A}(R^2 - R_0^2)$$

where k'' is the rate coefficient of surface reaction per unit area, M_B is the molecular weight of lysozyme, C_A is the reactant concentration, ρ_B is the density of a lysozyme crystal, and D_A is

Table 1
Surface rate equations used to simulate the crystal growth process.

Surface reaction	Rate equations
Adsorption r_a:	$K_0^+ \exp(\sigma)$
Desorption $r_d(i)$:	$K_0^+ \exp\left(\dfrac{\phi}{k_B T} - i\dfrac{E_{pb}}{k_B T}\right)$
Migration $r_m(i)$:	$K_0^+ \exp\left(\dfrac{\phi}{k_B T} - i\dfrac{E_{pb}}{k_B T} + \dfrac{E_{pb}}{2 k_B T}\right)$

the diffusion coefficient. The value of D_A is 10^5–10^6 cm^2/s (Kim and Myerson, 1996), and k'' can be considered as the growth rate of the lysozyme crystal in this study, which is 0.1–1 μm/min. Therefore, we can simply calculate t_{mt}/t_{rxn} from the preceding equations along with the approximated numbers for D_A and k'' as follows:

$$\frac{t_{mt}}{t_{rxn}} = \frac{k''}{2 D_A}(R + R_0) \tag{3}$$

where $t_{mt}/t_{rxn} \cong 10^{-11}$–$10^{-13}$. Therefore, it is now apparent that the crystal growth process is reaction-limited and thus is size-independent, and so is the dissolution process.

3.3. Crystal growth

In kMC simulations, the protein crystals are very compact without voids and overhangs due to the solid-on-solid model, which is assumed in this work. Additionally, along with the periodic boundary condition, we employed a square lattice model of length and width $N=30$ sites because no finite size effect is observed (Ke et al., 1998). Additionally, the following rate equations are used to simulate the crystal growth mechanisms (Durbin and Feher, 1991; Ke et al., 1998).

In Table 1, K_0^+ is the adsorption coefficient, i is the number of adjacent neighbors, E_{pb} is the average binding energy per bond, and ϕ is the total binding energy when a molecule is fully surrounded by neighbors (i.e., when $i=4$). Additionally, the fact that the migration rate is higher than the desorption rate is accounted for by multiplying an exponential factor into the desorption rate expression (Ke et al., 1998). To evaluate a set of E_{pb} and ϕ values for the (110) and (101) faces, open-loop kMC simulations are executed by adjusting model parameters to make the difference between the growth rates in the simulations and the experiments from literature very small.

3.4. Mass and energy balances

3.4.1. Mass balance
A constant crystal shape factor has been widely used to model three-dimensional (3-D) crystal growth, however, this factor usually depends on the supersaturation level in practice. The mass balance is developed by modeling the crystal shape as an aspect ratio of crystal heights into (110) and (101) directions. A variety of shape descriptors are available such as roundedness, 2-D area, convexity, length/width, and aspect ratio. Therefore, a careful selection is needed in order to quantify the crystal shape and use it in the controller design (Hentschel and Page, 2006; Pourghahramani and Forssberg, 2005).

The inlet and outlet flows and the fines trap, which are key components in the continuous crystallizer, are considered in the mass balance for the protein solute in the continuous phase. Therefore, the amount of the protein solute, C, that remains in the continuous phase can be approximated through the following

equation:

$$\frac{dC}{dt} = -\underbrace{\frac{\rho_c}{V_{MSMPR}}\frac{dV_{crystal}}{dt}}_{removed\ by\ crystals} + \underbrace{\frac{C_0}{\tau}}_{incoming\ flow} + \underbrace{\frac{\rho_c}{V_{MSMPR}}\frac{d\overline{V}_{fines}}{dt}}_{added\ by\ fines\ trap} - \underbrace{\frac{C}{\tau}}_{outgoing\ flow} \qquad (4)$$

where V_{MSMPR} is the crystallizer volume, τ is the residence time of the crystallizer, and $V_{crystal}$ is the total volume of crystals removed from the continuous phase considering the geometry of lysozyme crystals. In the kMC simulation, we have a constraint that the volume of crystals removed through the fines trap should not exceed 30% of the crystals leaving through the product stream. Initially, the residence time of a crystal is determined by the residence time distribution with a mean residence time of 1 hour. Then, this crystal will be checked every second and, when its size is less than the cut-off size, it will be removed through the fines trap with a probability of 50% (i.e., accounting for the efficiency of the fines trap). Therefore, the residence time is not explicitly considered for the operation of fines trap in the kMC simulations. However, in the controller, the moment models are solved in order to approximate the crystal volume distribution using the same residence time for both the product stream and the fines trap stream. We assume that the fines trap remove crystals of size $V_m(=8\ \mu m^3)$ or smaller. To this end, $\overline{V}_{fines}$ is newly introduced to indicate the total volume of crystals passed through the fines trap and dissolved. In Eq. (4), the first term represents the depletion of the solute concentration in the continuous phase due to crystallization. Then, the second and third terms stand for the incoming flow of fresh solution to the crystallizer and the incoming flow of a particle-free solution from the fines trap, respectively. The last term indicates the outflow from the crystallizer.

3.4.2. Energy balance

The energy balance accounts for the temperature change due to the enthalpy of crystallization, the heat transfer by manipulating the jacket temperature, and the heat transported in/out along the inflow/outflow as follows:

$$\frac{dT}{dt} = -\frac{\rho_c \Delta H_c}{\rho C_p V_{MSMPR}}\frac{dV_{crystal}}{dt} - \frac{U_c A_c}{\rho C_p V_{MSMPR}}(T - T_j) + \frac{T_{in} - T}{\tau} \qquad (5)$$

where T is the temperature inside the crystallizer, T_{in} is the inflow temperature, and T_j is the jacket temperature, $\rho_c = 1400\ mg/cm^3$ is the crystal density, $\Delta H_c = -44.5\ kJ/kg$ is the enthalpy of crystallization, $\rho = (1000 + C)\ mg/cm^3$ is the continuous phase solution density, $C_p = 4.13\ kJ/K\ kg$ is the specific heat capacity, $V_{MSMPR} = 1\ L$ is the continuous crystallizer volume, $A_c = 0.25\ m^2$ is the surface area of crystallizer wall, and $U_c = 500\ kJ/m^2\ h\ K$ is the heat transfer coefficient of crystallizer wall, which is usually smaller than that of a batch process. In practice, an appropriate cooling process is placed after the fines trap so that the changes in the crystallizer temperature caused by those streams are negligible.

In the kMC simulation, the residence time of a crystal is assumed to be distributed exponentially (Levenspiel, 1998) as follows:

$$\exp(-T_r/\tau) = RN$$

where T_r is the residence time of a crystal in the crystallizer, τ is the mean residence time, and RN is the random number generated between 0 and 1.

3.5. On-line imaging techniques for real-time measurement

As is mentioned previously, crystal shape can significantly affect the bioavailability of pharmaceutical products. Regardless, the direct characterization of particle shape has been limited to off-line techniques. For example, the PharmaVision System 830

(PVS830) has been widely used for the characterization of chord length distribution (CLD) and crystal shape distribution (CSD). To perform the image analysis, a sample has to be collected using a pipette and quickly placed on a sample tray under a high-speed video camera. However, this imaging technique has a number of issues. First, it cannot take images of particles as they actually exist in the crystallizer. Second, the sampling may alter the system condition and it leads to undesired dissolution, growth, and agglomeration of particles. Third, in the course of sample preparation through dilution, cooling, or heating, the particles may be significantly damaged before they are measured.

Motivated by the above reasons, new on-line in-process imaging techniques have been developed and released to the market such as PVM developed by Lasentec, which has been widely used to capture the size and shape distributions of crystals in crystallization processes. The PVM produces images of crystals which can be viewed through an external window. Through the PVM, the measurements of both CLD and CSD are available by taking images of a number of crystals. Moreover, images taken using PVM can be quickly verified through the comparison with other analytical equipments such as FBRM which is another widely used equipment using a focused beam of laser light to scan the size and shape of particles. As this light scans across those particles passing in front of the probe window, light is scattered in all directions and the light scattered back to the probe is used to calculate CLD and the number of crystals at every 30–40 s. Overall, PVM along with Lasentec FBRM provides new insight into crystallization processes by quantifying CLD, CSD, and crystal count. To this end, a new software program is developed to link PVM images with FBRM measurements (Calderon De Anda et al., 2005a, 2005b).

We note that the CLD and CSD are also influenced by system disturbances (i.e., particle orientation and noise in the system). Reflecting the presence of uncertainty in the kMC simulation, a noise is introduced to the measurement of CLD and CSD to account for the lack of knowledge of the direct measurements of actual particle distributions in practice. The noise is set to be 20% of its nominal value. In other words, when the measurements are sent to controller, they can be distorted up to 20% of their actual values. To obtain more precise measurements, the imaging techniques should be robust to the undesired noises present in the system. Furthermore, the development of high speed cameras can clarify the images which are sometimes poor due to the inconsistent distances of particles from the lens of cameras. Additionally, the high speed camera allows for a series of successive images of a particle with different orientations.

4. Population balance modeling

4.1. PBE of crystal volume distribution

In this section, we describe the profile of the crystal volume distribution with time in a continuous crystallizer with a fines trap accounting for nucleation and crystal growth as follows:

$$\frac{\partial n(V,t)}{\partial t} + G_{vol}\frac{\partial n(V,t)}{\partial V} = -\underbrace{\frac{n(V,t)}{\tau}}_{outflow} - \underbrace{\overline{h}(V)\frac{n(V,t)}{\overline{\tau}}}_{fines\ trap} + \underbrace{\delta(V-V_0)B(\sigma)}_{nucleation} \qquad (6)$$

where V denotes the crystal volume, t is the time, $\overline{\tau}$ is the residence time for the fines trap, $n(V,t)$ denotes the number of crystals with volume V at time t, $B(\sigma)$ is the nucleation rate, and dV/dt is the volumetric growth rate of crystals. The selection function for fines removal, $\overline{h}(V)$, is shown below:

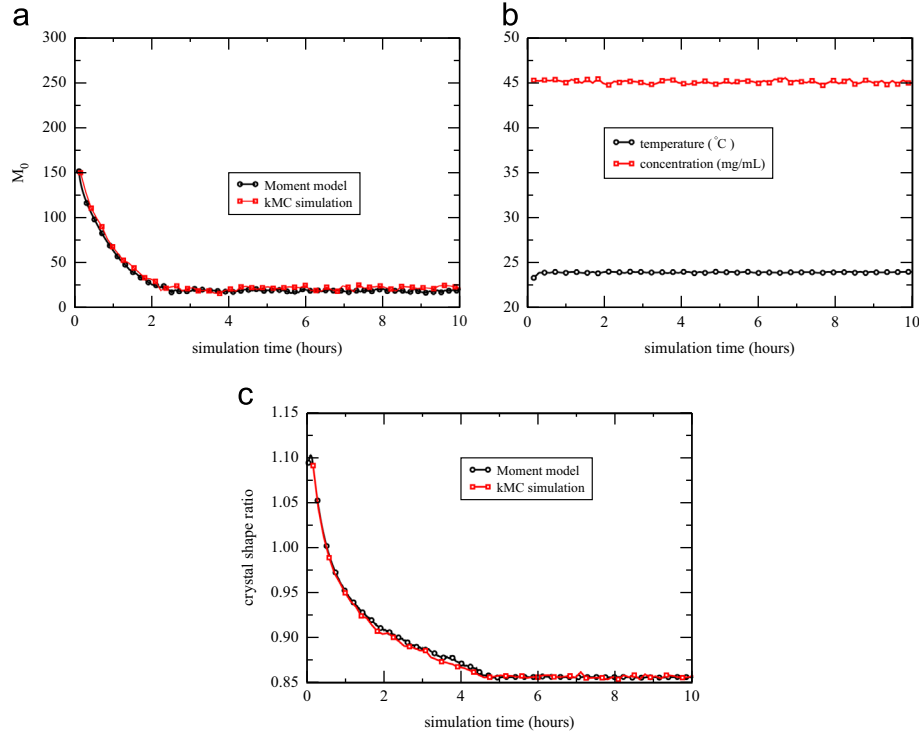$$\overline{h}(V) = \begin{cases} 1 & for\ V \leq V_m \\ 0 & for\ V > V_m \end{cases}$$

Fig. 2. Profiles of the open-loop simulation of number of crystals, crystallizer temperature, protein solute concentration, and average crystal shape for the crystallization of tetragonal lysozyme protein at pH=4.5. (a) Number of crystals (M_0), (b) temperature and concentration and (c) crystal shape (α).

where V_m is the cut-off size of a fines trap. Approximating the total volume of the entire lysozyme crystal population as $V(t) \sim M_0(t)\langle h_{110}(t)\rangle^2 \langle h_{101}(t)\rangle$, we can compute the volume growth rate G_{vol} by calculating the volumetric growth rate of crystals, dV/dt, through the following equation:

$$G_{vol} = \frac{dV(t)}{dt} = \frac{dM_0(t)\langle h_{110}(t)\rangle^2 \langle h_{101}(t)\rangle}{dt}$$
$$= M_0(t)\left(2\frac{d\langle h_{110}\rangle}{dt}\langle h_{110}(t)\rangle\langle h_{101}(t)\rangle + \frac{d\langle h_{101}\rangle}{dt}\langle h_{110}(t)\rangle^2\right) + \frac{dM_0}{dt}\langle V(t)\rangle$$
(7)

where the right hand side is readily available from the measurements along with Eqs. (18) and (19), which will be discussed in Section 5.1. In the kMC simulation, which models an actual crystallizer, $dV_{crystal}/dt$ and $d\overline{V}_{fines}/dt$ are computed by summing the total volume of crystals changed/removed over a sampling time. Furthermore, $d\overline{V}_{fines}/dt$ is approximated by summing the number of crystals whose sizes are less than the cut-off size because the statistics (e.g., mean and standard deviation) of the crystal volume distribution is available from the measurements along with Eqs. (13) and (14). Additionally, Eq. (6) can be rewritten with the addition of an appropriate boundary condition as is shown below:

$$\frac{\partial n(V,t)}{\partial t} + \frac{n(V,t)}{\tau} + \overline{h}(V)\frac{n(V,t)}{\overline{\tau}} + G_{vol}\frac{\partial n(V,t)}{\partial V} = 0$$
(8)

$$n(0,t) = \frac{B(\sigma)}{G_{vol}}$$

Further details regarding the derivation of the boundary condition can be found in our previous work (Kwon et al., 2013b).

4.2. Moment models

The numerical computation of the crystal volume distribution using Eq. (6) is computationally expensive and not readily

accessible in general because of the complexity in the PBE. To deal with this issue, the method of moments is applied to Eq. (6) in order to derive moment models. Specifically, the jth moment is defined as follows:

$$M_j = \int_o^\infty V^j n(V,t)\, dV$$
(9)

Along with the balance equations of Eqs. (4) and (5), the three leading moments are used to approximate the dominant behavior of the nucleation and crystal growth in a continuous crystallizer with a fine trap. For more details regarding the derivation of the following three moment models, the reader may want to refer to our earlier work (Kwon et al., 2013b).

Zeroth moment: It describes the rate of change of the total number of crystals with time:

$$\frac{dM_0}{dt} = B(\sigma) - \frac{M_0}{\tau} - \int_0^{V_m} \frac{n(V,t)}{\overline{\tau}}\, dV$$
(10)

where $B(\sigma)$ is justified by the boundary condition of Eq. (8). On the right hand side, the term with the integral indicates the number of crystals below the cut-off size of the fine trap and it can be evaluated from the measurement of the crystals where the statistics of size and shape distributions are available (e.g., mean and standard deviation).

First moment: It describes the rate of change in the total crystal volume with time:

$$\frac{dM_1}{dt} = G_{vol}M_0 - \frac{M_1}{\tau} - \int_0^{V_m} V\frac{n(V,t)}{\overline{\tau}}\, dV$$
(11)

Second moment: It describes the rate of change in the volume square of the entire crystal population with time:

$$\frac{dM_2}{dt} = 2G_{vol}M_1 - \frac{M_2}{\tau} - \int_0^{V_m} V^2\frac{n(V,t)}{\overline{\tau}}\, dV$$
(12)

When a fines trap is not used (i.e., $\overline{h}(V) = 0$), the first three moment equations and the mass and energy balance equations,

Eqs. (4) and (5), constitute a closed set of differential equations. However, the set of moment models above does not close owing to the classification function, $\bar{h}(V)$, for the fines trap. In order to close the set of moment equations and the balance equations, $n(V, t)$ is assumed to follow a normal distribution as follows:

$$n(V, t) = \frac{1}{\sigma_N \sqrt{2\pi}} \exp\left(-\frac{(V - \mu)^2}{2\sigma_N^2} \right) \tag{13}$$

where μ is the mean of crystal volume distribution, and σ_N is its standard deviation. They can be linked to the first three moments through the expressions below:

$$\mu = \frac{M_1}{M_0}, \quad \sigma_N = \sqrt{\frac{M_2}{M_0} - \mu^2} \tag{14}$$

The volume distribution of crystals obtained from the kMC simulations at $t = 1$ h has been presented in Fig. 5 verifying the normal distribution assumption. We should note that the volume distribution may show a biased bimodal behavior due to a burst of nucleation at a higher supersaturation level, however the assumption is still acceptable as it would not affect the controller performance significantly. Using Eqs. (13) and (14), we can numerically integrate the fines trap term in the moment models, Eqs. (10)–(12).

5. Open-loop simulation results

Analytically solving the PBE for the profiles of the crystal shape and size distributions is equivalent to executing multiple kMC simulations over an infinite number of lattice sites along with the consideration of balance equations. In this work, the kMC simulation is further developed from the previous work (Kwon et al., 2013b) to model a continuous crystallization along with the dissolution of small crystal fines. In particular, $N = 30$ is used for the number of lattice sites, because no finite size effect is observed in the kMC simulations with lattice sites more than $N = 30$ by Ke et al. (1998).

In Fig. 2, the profiles of the number of crystals (M_0), the average crystal shape $\langle \alpha \rangle$, and the crystallizer temperature and the solute concentration obtained from the moment models (cf. Eqs. (10)–(12)), are compared with those of the kMC simulation. The number of crystals increases in the beginning until it reaches a steady-state because the simulation begins with a crystal-free solution. Afterward, the variables remain constant reflecting the steady-state operation of the continuous crystallizer. For example, the solute concentration remains constant at 45 mg/mL. Overall, the result obtained by the reduced moment models shows a very good match with that of the kMC simulation.

Sometimes, highly oscillatory behavior takes place in the crystallizer as a result of the competing interplay between the nucleation and crystal growth. As is described in Chiu and Christofides (1999, 2000), it is mainly caused by the nonlinearity in the nucleation rate (i.e., exponential dependence on supersaturation) as compared to that in the growth rate (i.e., linear dependence on supersaturation) which causes the following scenario: the amount of fines progressively decreases as the supersaturation drops due to the consumption of protein solute by the crystal growth as well as the nucleation. As a consequence, the supersaturation level drops to a point where the nucleation rate begins to drop drastically, and thus no further nucleation occurs and the present small crystal fines grow into coarse crystals. Then, the supersaturation level starts to build up due to the absence of the nucleation until it reaches a point where a burst in the nucleation occurs with the production of a large number of fines. In this study, however, this oscillatory behavior of crystal
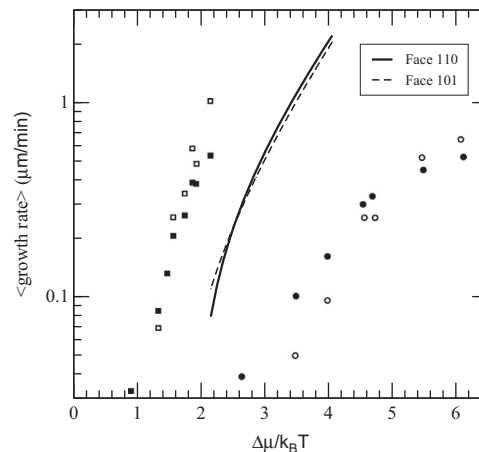

Fig. 3. The solid and dashed lines show the growth rates for the kMC model on the (110) and (101) faces, respectively, at $C = 45$ mg/mL and 4% NaCl. The ($\bullet$)/ ($\circ$) represent the growth rates for (101) and (110) faces with 3.5% NaCl and the ($\blacksquare$) and ($\square$) represent the growth rates with 5% NaCl at pH=4.6, which both are taken from Durbin and Feher (1986).
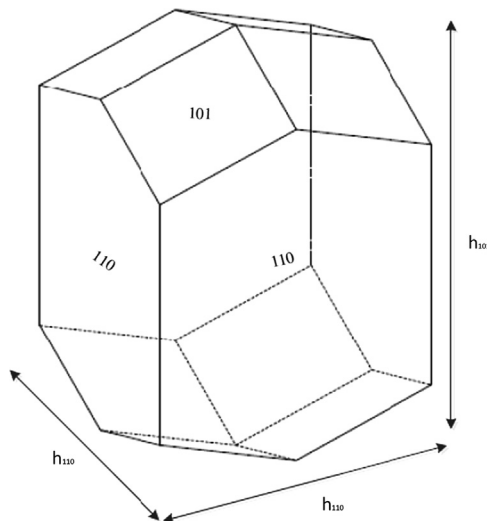

Fig. 4. Geometry of tetragonal lysozyme crystal.

size, number of crystals, supersaturation level, and so on, is not observed because the working range (e.g., supersaturation level) is relatively high so that the nucleation rate shows a linear dependence on the supersaturation level (cf. the regime where $\sigma \geq 3.11$ in Eq. (1)).

In Fig. 3, $(\phi/k_B, E_{pb}/k_B)_{110} = (1077.26K, 227.10K)$ and $(\phi/k_B, E_{pb}/k_B)_{101} = (800.66K, 241.65K)$, and $K_o^+ = 0.211$ s^{-1} are used for the open-loop simulation, and the crystal growth rates at 4%(w/v) NaCl and pH=4.5 have been compared along with the experimental results (Durbin and Feher, 1986) at 3.5% and 5.0% NaCl, respectively.

5.1. Modeling of crystal shape distribution from measurements

In kMC simulation, the 3-D crystal growth is modeled along the two representing characteristic lengths, h_{110} and h_{101}, as they are shown in Fig. 4. Furthermore, the growth rates, $G_{110}(\sigma)$ and $G_{101}(\sigma)$, from Fig. 3 are approximated by the following polynomial expressions as a function of supersaturation:

$$G_{110}(\sigma) = 0.1843 \times \sigma^3 - 1.1699 \times \sigma^2 + 2.8885 \times \sigma - 2.5616$$
$$G_{101}(\sigma) = 0.1893 \times \sigma^3 - 1.2264 \times \sigma^2 + 2.9887 \times \sigma - 2.5348 \tag{15}$$

with units μm/min. These polynomials show a very good fit with an R^2 value of nearly 1. Additionally, we note here that the growth rate ratio, $G_{110}(\sigma)/G_{101}(\sigma)$, is equal to the aspect ratio between the two heights at the steady-state.

The measurements of the mean of CLD, $\langle h \rangle$, and the mean of CSD, $\langle \alpha \rangle$, are available through the measurements of the crystals inside the crystallizer. By the definition of CLD and CSD, we can link $\langle h \rangle$ and $\langle \alpha \rangle$ with $\langle h_{110} \rangle$ and $\langle h_{101} \rangle$ as follows:

$$\langle \alpha \rangle \approx \frac{\langle h_{110} \rangle}{\langle h_{101} \rangle} \quad \frac{\langle h_{110} \rangle + \langle h_{101} \rangle}{2} \approx \langle h \rangle \quad (16)$$

In general, it is nearly impossible to obtain the in-process online measurements of the average crystal height in each direction, $\langle h_{110} \rangle$ and $\langle h_{101} \rangle$. Instead, we will approximate the average heights on each face with the measurements of $\langle h \rangle$ and $\langle \alpha \rangle$, which are available through the PVM and FBRM:

$$\langle h_{101} \rangle = \frac{2\langle h \rangle}{\langle h \rangle + 1} \quad \langle h_{110} \rangle = \frac{2\langle h \rangle \langle \alpha \rangle}{\langle h \rangle + 1} \quad (17)$$

We additionally note here that $M_0(t)$ is the number of crystals inside the crystallizer, whose measurement is also available through the FBRM. Then, we will make predictions of the average height of the crystal face (110) through the following ODE:

$$\frac{d\langle h_{110} \rangle}{dt} = G_{110}(\sigma) - \frac{B(\sigma)V_{MSMPR}\langle h_{110}(t) \rangle}{M_0(t)} \quad (18)$$

In the same manner, the average height of the crystal face (101) can be predicted as follows:

$$\frac{d\langle h_{101} \rangle}{dt} = G_{101}(\sigma) - \frac{B(\sigma)V_{MSMPR}\langle h_{101}(t) \rangle}{M_0(t)} \quad (19)$$

By combining the equations above, we can predict the average crystal shape in the following way:

$$\langle \alpha \rangle \approx \frac{\langle h_{110}(t) \rangle}{\langle h_{101}(t) \rangle} \quad (20)$$

6. Model predictive control of crystal shape in continuous crystallization

6.1. Real-time feedback control of crystal shape

In order to control the crystal shape by manipulating the jacket temperature in the crystallizer, a control scheme inspired by our previous work (Kwon et al., in press, 2013b) is proposed in this work. The incoming stream to the crystallizer is a crystal-free solution with a protein solute concentration $C = 45$ mg/mL at a flow rate of Q. At the same rate, the crystals are removed from the crystallizer along the outgoing stream whose solute concentration is identical to that in the continuous phase in the crystallizer. In the simulation, it is assumed that CLD and CSD are measured in real time and the measurements are used in order to estimate the average aspect ratio $\langle \alpha \rangle = \langle h_{110} \rangle / \langle h_{101} \rangle$ as is shown in Eq. (20). This can be achieved in practice using the aforementioned imaging techniques such as PVM and FBRM. Additionally, a noise with 20% fluctuation of the nominal value is introduced to account for the incompleteness of the currently available measurement techniques. Along with the noise, these measurements are sent to a controller which computes the optimal jacket temperature to control the crystal shape $\langle \alpha \rangle$ to a desired value. For example, if a higher aspect ratio (elongated prism) is desired, the controller lowers the jacket temperature and thus the crystallizer temperature gets lowered to a moderate value where the production of a desired shape is favored.

6.2. Model predictive formulation

A continuous crystallization process with a fines trap is modeled through a set of moment models along with the mass and energy balances in order to describe the evolution of the crystal size and shape distributions with time. Through the modeling of the crystallization process, we design a model predictive controller to regulate the shape and size distributions of crystals nucleated along the process. Minimizing the sum of the deviation of the average crystal aspect ratio and growth rate ratio from a desired value, and penalizing the control action, is chosen as a control objective, and the jacket temperature is used as the manipulated input. In the continuous crystallizer, the proposed control design can be applied to the case of multi-inputs (Aldabaibeh et al., 2009; Weber et al., 2008; Müller et al., 2011; Müller and Ulrich, 2011) such as the solute concentration in the feed stream and the flow rate of the fines trap stream. Additionally, the measurements of the solute concentration, CLD and CSD, are assumed to be available at every sampling time ($\Delta = 40$ s). In particular, the uncertainty in the measurement of the solute concentration is reflected in the simulation by introducing the fluctuation of the concentration through the way described in our earlier work (Kwon et al., 2013b).

In the control formulation, a couple of limitations are taken into account in the form of constraints along with the mass and energy balances (Eqs. (4) and (5)). A limit on the range of the crystallizer temperature, $4\,^\circ C \leq T \leq 25\,^\circ C$, is imposed to prevent lysozyme proteins from being damaged. Additionally, there is a limit on the rate of the jacket temperature change, $2.0\,^\circ C/min$, to account for actuator limitations. The cost function of the optimal control problem has penalties on both the deviation of $\langle \alpha \rangle$ and the G_{110}/G_{101} from its desired crystal shape, α_{set}, as well as penalty on the control input. Furthermore, by adjusting the coefficients between the penalties on the off-spec production of the crystal shape and the control action, respectively, we can prevent unnecessarily aggressive control action. For example, when the penalty on the off-spec of the crystal shape is more weighted, the control action will be eager to reach a desired growth condition as soon as possible, subject to other constraints. On the other hand, when the penalty on the control actions is more weighted, the controller will achieve the desired condition more slowly. Furthermore, we note that the proposed control scheme can be easily extended to consider the case of multiple inputs including the flow rate of streams to the crystallizer and the fines trap. However, it is outside the scope of this work and will be further considered with details in the future. The MPC has the following form:

$$\underset{T_{j,1},\ldots,T_{j,i},\ldots,T_{j,p}}{\text{minimize}} \quad \sum_{i=1}^{p} w_1 \left(\frac{\langle \alpha(t_i) \rangle - \alpha_{set}}{\alpha_{set}} \right)^2$$

$$+ w_2 \left(\frac{\frac{G_{110}(\sigma(t_i))}{G_{101}(\sigma(t_i))} - \alpha_{set}}{\alpha_{set}} \right)^2 + w_3 \left(\frac{T_{j,i+1} - T_{j,i}}{T_{j,i+1}} \right)^2$$

subject to $\quad 4\,^\circ C \leq T_i \leq 25\,^\circ C \quad \left| \frac{T_{j,i+1} - T_{j,i}}{\Delta} \right| \leq 2\,^\circ C/min$

$$G_{110}(\sigma) = 0.1843 \times \sigma^3 - 1.1699 \times \sigma^2 + 2.8885 \times \sigma - 2.5616$$

$$G_{101}(\sigma) = 0.1893 \times \sigma^3 - 1.2264 \times \sigma^2 + 2.9887 \times \sigma - 2.5348$$

$$\frac{dM_0}{dt} = B(\sigma) - \frac{M_0}{\tau} - \int_0^{V_m} \frac{n(V,t)}{\overline{\tau}}\,dV$$

$$\frac{dM_1}{dt} = G_{vol}M_0 - \frac{M_1}{\tau} - \int_0^{V_m} V\frac{n(V,t)}{\overline{\tau}}\,dV$$

$$\frac{dM_2}{dt} = 2G_{vol}M_1 - \frac{M_2}{\tau} - \int_0^{V_m} V^2\frac{n(V,t)}{\overline{\tau}}\,dV$$

$$\frac{dC}{dt} = -\frac{\rho_c}{V_{MSMPR}}\frac{dM_1}{dt} + \frac{C_0}{\tau} + \frac{\rho_c}{V_{MSMPR}}\frac{d}{dt}\left(\int_0^{V_m} V\frac{n(V,t)}{\overline{\tau}}dV\right) - \frac{C}{\tau}$$

$$\frac{dT}{dt} = -\frac{\rho_c \Delta H_c}{\rho C_p V_{MSMPR}}\frac{dM_1}{dt} - \frac{U_c A_c}{\rho C_p V_{MSMPR}}(T - T_j) + \frac{T_{in} - T}{\tau}$$

$$\frac{d\langle h_j\rangle}{dt} = G_j(\sigma) - \frac{B(\sigma)V_{MSMPR}\langle h_j(t)\rangle}{M_0(t)}$$

$$\langle\alpha(t)\rangle \approx \frac{\langle h_{110}(t)\rangle}{\langle h_{101}(t)\rangle}, \quad \sigma = \ln(C/s)$$

$$i = 1, 2, \ldots, p \quad \text{and} \quad j \in \{110, 101\} \tag{21}$$

where $p = 10$ is the number of prediction steps, w_1, w_2, w_3 are the weighted coefficients, $t_i = t + i\Delta$ is the time of the ith prediction step, $T_{j,i}$ is the jacket temperature of the ith prediction step, respectively. At every sampling time, the first three moments and the balance equations are updated along with the rate of change of the average height on each face j (cf. Eqs. (18)–(20)). Then, the first value of the set of optimal jacket temperatures ($T_{j,1}, T_{j,2}, \ldots, T_{j,p}$) is applied to the system over the following sampling time. Then, a set of new measurements for CLD, CSD, protein solute concentration, and the number of crystals is collected from the kMC simulation, and a new set of optimal jacket temperatures is obtained by re-solving Eq. (21) based on the new measurements. In the work by Shi et al. (2005), empirical expressions are used to model the evolution of crystallization including both nucleation and crystal growth. However, in this work, the kMC simulations are used for more realistic modeling of a continuous crystallization process based on the rate equations described in Table 1. Additionally, the readers who are interested in the robust model predictive control of a crystallization process may want to refer to Shi et al. (2006) and Chiu and Christofides (2000).

7. Continuous crystallization under closed-loop operation

In Fig. 3, it is shown that the range of growth rate ratio $G_{110}(\sigma)/G_{101}(\sigma)$ ranges from 0.7 to 1.1. Two desired crystal morphologies, $\langle\alpha\rangle = 1.18$ and $\langle\alpha\rangle = 0.86$, are chosen as desired set-points in the closed-loop simulations where the former and the latter represent crystals with more elongated into (110) and (101) directions, respectively.

Due to the dependency of the nucleation rate on the supersaturation level, an abrupt change in the crystallizer temperature in an effort to achieve a desired optimal temperature may result in a biased nucleation. The biased nucleation is cumbersome, because the crystals nucleated in the earlier stage can go through undesired growth condition, and subsequently it leads to poor controller performance. In our earlier work (Kwon et al., 2013a), it was shown that when the desired shape is $\langle\alpha\rangle = 0.85$ and the initial temperature is $T_0 = 5\,°C$, the corresponding optimal temperature is $\sim 23.7\,°C$ and the nucleation of $\sim 34\%$ of the entire crystal population occurs within the first $\sim 5\%$ of the entire 4000 s batch process. In a continuous crystallizer, however, the issue with the biased nucleation can be avoided by simply operating a system at a steady-state, where the nucleation rate remains constant.

A steady-state crystallizer temperature is determined by the interplay among the inflow, crystallizer, and jacket temperatures as is shown in the energy balance equation (cf. Eq. (5)). Similar to a batch process, an initial crystallizer temperature, which is equivalent to the inflow temperature, is important to the controller performance. For example, if an inflow temperature is too far from an optimal temperature, it results in a discrepancy of a steady-state temperature from an optimal temperature due to the limited heat transfer rate. The difference can be more critical to the controller performance when the production of crystals with a lower set-point value is desired, because crystals with a low $\langle\alpha\rangle$ are usually produced at a high temperature level where the crystal
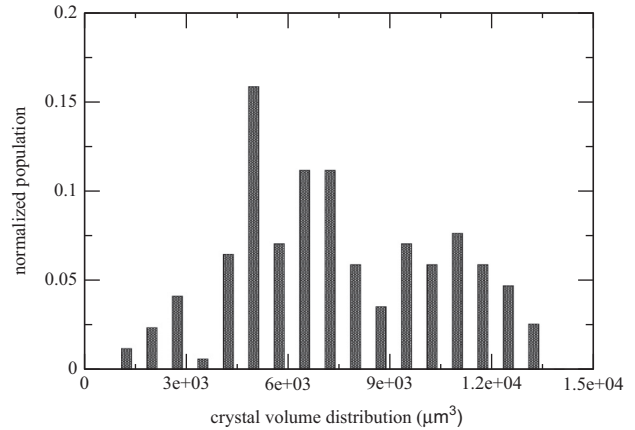

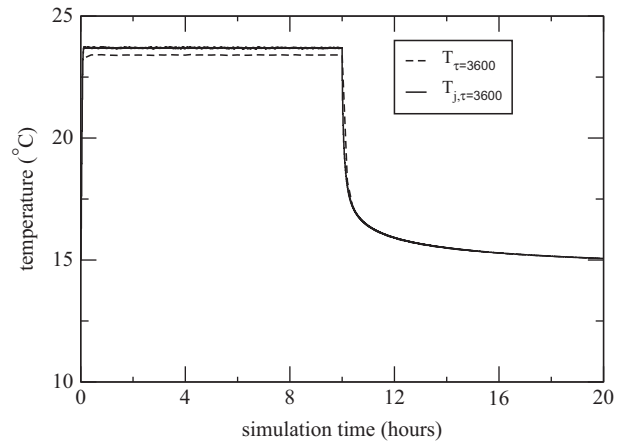Fig. 5. The normalized crystal volume distribution obtained from the kMC simulations at $t = 1$ h.

Fig. 6. The profile of crystallizer temperature (T) and jacket temperature at $\tau = 3600$ s under MPC for the initial crystal shape set-point value, $\langle\alpha\rangle = 0.86$. After $t = 10$ h, the set-point is changed to $\langle\alpha\rangle = 1.1$.
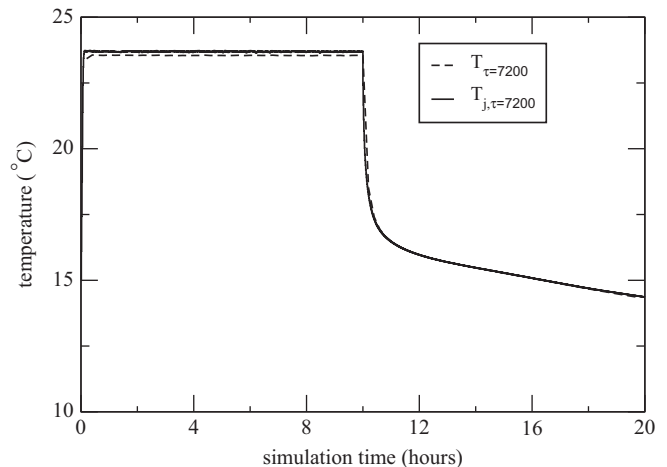

Fig. 7. The profile of crystallizer temperature (T) and jacket temperature at $\tau = 7200$ s under MPC for the initial crystal shape set-point value, $\langle\alpha\rangle = 0.86$. After $t = 10$ h, the set-point is changed to $\langle\alpha\rangle = 1.1$.

morphology is very sensitive to the small changes in the supersaturation level (Kwon et al., 2013a). We can achieve a better controller performance through the following approach: First, adjusting inflow temperature appropriately can enhance the performance of the proposed MPC by achieving a crystallizer temperature, which is closer to an optimal temperature. Second,
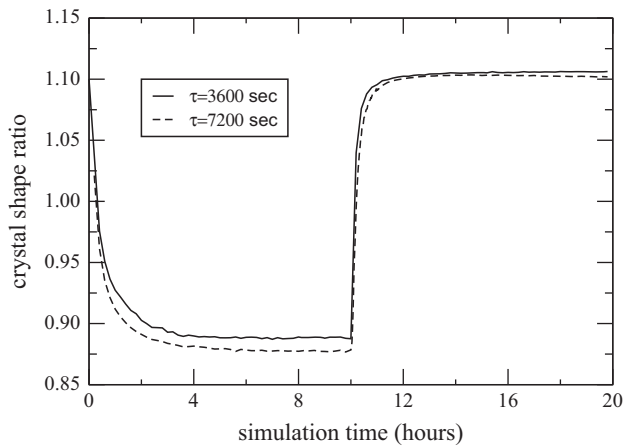
Fig. 8. The profile of the average crystal shape $\langle\alpha\rangle$ under MPC for the initial crystal shape set-point value, $\langle\alpha\rangle = 0.86$. After $t = 10$ h, the set-point is changed to $\langle\alpha\rangle = 1.1$.
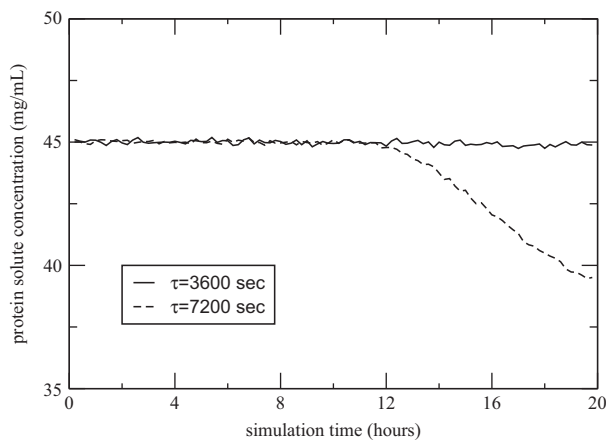

Fig. 10. The profile of the average number of crystal (M_0) with time under MPC for the initial crystal shape set-point value, $\langle\alpha\rangle = 0.86$. After $t = 10$ h, the set-point is changed to $\langle\alpha\rangle = 1.1$.

Fig. 9. The profile of solute concentration (C) under MPC for the initial crystal shape set-point value, $\langle\alpha\rangle = 0.86$. After $t = 10$ h, the set-point is changed to $\langle\alpha\rangle = 1.1$.

Fig. 11. The profile of the average volume (M_1/M_0) of the crystal population in Fig. 10 with time under MPC for the initial shape set-point value, $\langle\alpha\rangle = 0.86$. After $t = 10$ h, the set-point is changed to $\langle\alpha\rangle = 1.1$.

the heat transfer rate can be increased by using a material with a higher overall heat transfer coefficient, U_c, and thus the discrepancy can be reduced. Third, the choice of an appropriate residence time is also important because the crystallizer temperature at a steady-state is influenced by the residence time (cf. Eq. (5)). For example, if the residence time is too small (e.g., less than an hour), crystals with desired shape and size distributions cannot be produced because crystals do not stay inside a crystallizer for a sufficient amount of time. On the other hand, if the residence time is too large, the dynamics of a continuous process becomes similar to that of a batch process in that crystals stay for a very long time inside a crystallizer, and thus severe drop in the protein solute concentration is observed. Specifically, it is shown in Figs. 6–8 that increasing the residence time will enable the system to reach a steady-state temperature, which is much closer to a desired value, and thus will result in a narrow range of desired crystal shape distributions. Moreover, when $\tau \geq 2$ h, significant concentration drop was observed and thus simply lowering temperature is not sufficient to maintain a supersaturation level to an optimal value, and thus it leads to a poor controller performance, as is shown in Figs. 8 and 9.

In Figs. 6–11, the foregoing analysis is demonstrated through the profiles of the crystallizer temperature, the jacket temperature, the protein solute concentration, the average crystal volume, and the average crystal shape along the simulation at different residence times. Initially, the jacket temperature is simply increased to the optimal value by the proposed MPC as is shown by Figs. 6
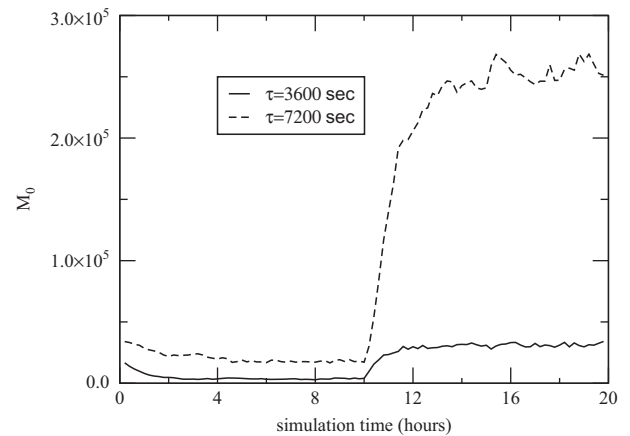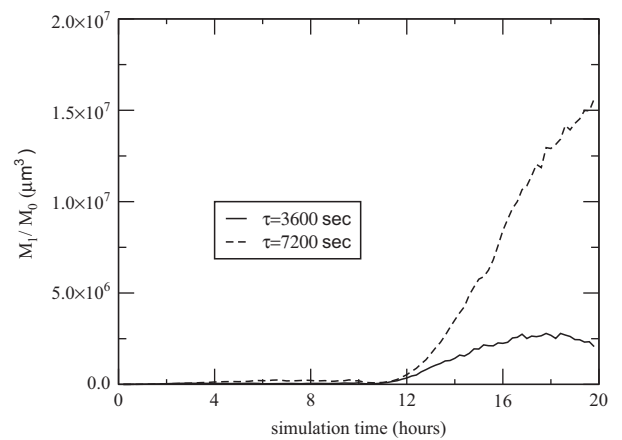
and 7, and the crystallizer temperature is driven by the jacket temperature accordingly. A burst of crystal nucleation, which is caused by a high supersaturation level, is appropriately suppressed through a fines trap where most of the small crystal fines are destructed by adjusting the temperature, and thereby dissolution rates. As a result, large crystals grow larger and small crystal fines are dissolved back to the continuous phase. However, we note that no significant rise in the solute concentration is observed because typically the fraction of fines removed is 10^{-6}–10^{-5} of the production rate on a mass basis.

In order to test the response time of the MPC toward a change in the desired set-point, after 10 h, the set-point is changed from $\langle\alpha\rangle = 0.86$ to $\langle\alpha\rangle = 1.1$ where a high supersaturation level is favored for the production of crystals with a shape more elongated into (110) direction. As a result, the crystallizer temperature is decreased to $T = 15.0\,^\circ$C, owing to the jacket temperature computed by MPC, as is shown in Figs. 6 and 7. Specifically, for the closed-loop simulation of $\tau = 1$ h, the crystallizer temperature remains constant once the system reaches a new steady-state for $\langle\alpha\rangle = 1.1$. However, for $\tau = 2$ h, the jacket temperature keeps decreasing to counteract the severe protein solute concentration drop and maintain a desired supersaturation level. In both cases above, the MPC is able to drive the crystal population to a desired value as it is shown in Fig. 12. Additionally, as we change the set-point from $\langle\alpha\rangle = 0.86$ to $\langle\alpha\rangle = 1.1$, it is shown in Fig. 13 that it takes about 2 h for the system to reach the new steady-state for $\tau = 2$ h.
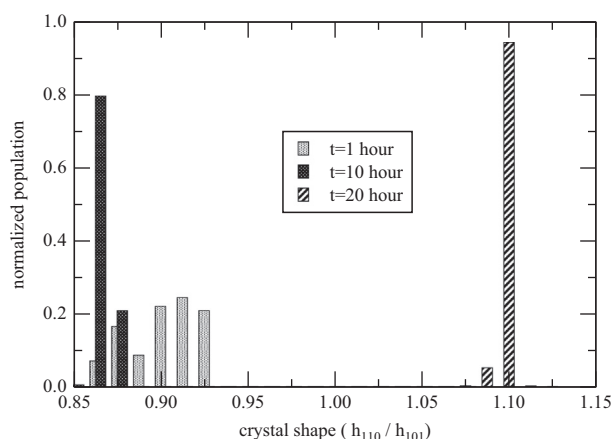
Fig. 12. The normalized crystal shape distribution at three different times during the simulation at $\tau = 7200$ s under MPC for the initial crystal shape set-point value, $\langle \alpha \rangle = 0.86$. After $t = 10$ h, the set-point is changed to $\langle \alpha \rangle = 1.1$. The histograms are obtained by averaging 10 independent kMC simulations where the standard deviation for $t = 1$, $t = 10$, and $t = 20$ h are 0.019, 0.003, and 0.002, respectively.
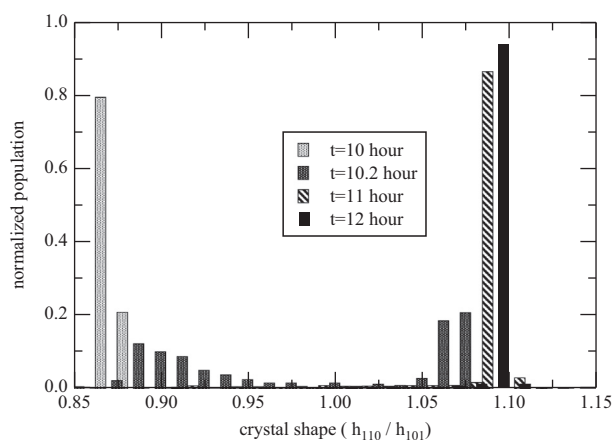

Fig. 13. The normalized crystal shape distribution at four different times during the transition period ($t = 10$–12 h) in the simulation under MPC at $\tau = 7200$ for the crystal shape set-point change from $\langle \alpha \rangle = 0.86$ to $\langle \alpha \rangle = 1.1$. The histograms are obtained by averaging 10 independent kMC simulations where the standard deviation for $t = 10$, $t = 10.2$, $t = 11$, and $t = 12$ h are 0.003, 0.008, 0.025, and 0.011, respectively.

Considering the fact that the mean residence time is 2 h, a response time of about 2 h is reasonable. Therefore, it verifies that the proposed MPC responds promptly to the change in the set-point, the severe concentration drop, and the system disturbances in an effort for the production of crystals with a desired morphology. Furthermore, the system's response time toward the set-point change can be even shorter when we use a short residence time, because the crystals with an undesired shape will exit the crystallizer quickly. We can also use an actuator with a higher limitation on the jacket temperature change, which will allow for the system to reach the optimal jacket temperature value faster.

In conclusion, the MPC with a fines trap is able to drive the crystal population to a desired shape distribution by appropriately dealing with the undesired effects such as the biased nucleation, disturbances, and the mismatch of moment models as demonstrated by Figs. 8 and 12. It should be noted that the controller performance of using multiple prediction steps does not show further improvement in terms of controller performance, because the control action is dominated by a constraint on the rate of temperature change. Therefore, the controller performance can be further improved by adjusting the constraint on the rate of change

of the manipulated input (i.e., jacket temperature) so that the system takes more aggressive actions. Additionally, compared to a batch process, a continuous process can achieve a low polydispersity easier for the following two reasons. First, the fines trap removes most of the small crystal fines whose sizes are less than the set cut-off size, and this allows for the remaining crystals to grow larger. Second, once the system reaches its steady-state in the continuous crystallization, an optimal condition for the production of crystals with a desired shape can be maintained until the process is terminated.

8. Conclusions

Initially, we presented the modeling of the nucleation, and crystal growth in a continuous crystallization process with a fines trap through kinetic Monte Carlo (kMC) simulation. The simulation of a fines trap was modeled through a classification function which indicates a selection curve for fines dissolution in the continuous crystallizer. In addition to the solute depletion and the temperature change in the continuous phase by crystallization, the interplay of inflow/outflow in the continuous crystallizer was included in the mass and energy balance equations. To deal with a real-time implementation issue of a controller based on PBM, moment models were developed to describe the dominant dynamic behavior of the continuous crystallization along with a fines trap. Subsequently, the three leading moments were used along with the balance equations in order to design a model predictive controller.

The simulation results demonstrated that the crystal growth at a steady-state operation was successfully regulated by properly adjusting the jacket temperature. The MPC also suppressed the influence of the biased nucleation, the disturbances in the measurements, and the sudden change in the desired operating environment (i.e., changes in the desired set-point value). Additionally, the measurements of CSD and CLD through FBRM and PVM, respectively, were assumed to be available from the kMC simulation. Compared to a batch process, crystals with a low polydispersity can be produced due to the fines trap as it dissolves most of the fines whose volumes are less than 1 μm^3 in the crystallizer. We can reduce the response time of the system toward the sudden set-point change by using a higher flow rate. Furthermore, using an actuator with a higher limitation on the jacket temperature change can allow for the system to respond quickly and reach the optimal jacket temperature value faster.

References

Aldabaibeh, N., Jones, M.J., Myerson, A.S., Ulrich, J., 2009. The solubility of orthorhombic lysozyme chloride crystals obtained at high pH. Cryst. Growth Des. 9, 3313–3317.

Alvarez, A., Singh, A., Myerson, A.S., 2011. Crystallization of cyclosporine in a multistage continuous MSMPR crystallizer. Cryst. Growth Des. 11, 4392–4400.

Bortz, A.B., Kalos, M.H., Lebowitz, J.L., 1975. New algorithm for Monte Carlo simulation of Ising spin systems. J. Comput. Phys. 17, 10–18.

Cacioppo, E., Munson, S., Pusey, M.L., 1991. Protein solubilities determined by a rapid technique and modification of that technique to a micro-method. J. Cryst. Growth 110, 66–71.

Cacioppo, E., Pusey, M.L., 1991. The solubility of the tetragonal form of hen egg white lysozyme from pH 4.0 to 5.4. J. Cryst. Growth 114, 286–292.

Calderon De Anda, J., Wang, X.Z., Lai, X., Roberts, K.J., 2005a. Classifying organic crystals via in-process image analysis and the use of monitoring charts to follow polymorphic and morphological changes. J. Process Control 15, 785–797.

Calderon De Anda, J., Wang, X.Z., Roberts, K.J., 2005b. Multi-scale segmentation image analysis for the in-process monitoring of particle shape with batch crystallisers. Chem. Eng. Sci. 60, 1053–1065.

Chen, J., Sarma, B., Evans, J.M., Myerson, A.S., 2011. Pharmaceutical crystallization. Cryst. Growth Des. 11, 887–895.

Chiu, T., Christofides, P.D., 1999. Nonlinear control of particulate processes. AIChE J. 45, 1279–1297.

Chiu, T., Christofides, P.D., 2000. Robust control of particulate processes using uncertain population balances. AIChE J. 46, 266–280.

Christofides, P.D., Armaou, A., Lou, Y., Varshney, A., 2008. Control and Optimization of Multiscale Process Systems. Birkhäuser, Boston.

Dai, J., Kanter, J.M., Kapur, S.S., Seider, W.D., Sinno, T., 2005. On-lattice kinetic Monte Carlo simulations of point defect aggregation in entropically influenced crystalline systems. Phys. Rev. B 72, 134102.

Dai, J., Seider, W.D., Sinno, T., 2008. Coarse-grained lattice kinetic Monte Carlo simulation of systems of strongly interacting particles. J. Chem. Phys. 128, 194705.

Durbin, S.D., Feher, G., 1986. Crystal growth studies of lysozyme as a model for protein crystallization. J. Cryst. Growth 76, 583–592.

Durbin, S.D., Feher, G., 1991. Simulation of lysozyme crystal growth by the Monte Carlo method. J. Cryst. Growth 110, 41–51.

El-Farra, N.H., Chiu, T., Christofides, P.D., 2001. Analysis and control of particulate processes with input constraints. AIChE J. 47, 1849–1865.

Forsythe, E.L., Nadarajah, A., Pusey, M.L., 1999. Growth of (101) faces of tetragonal lysozyme crystals: measured growth-rate trends. Acta Cryst. D 55, 1005–1011.

Galkin, O., Vekilov, P.G., 1999. Direct determination of the nucleation rates of protein crystals. J. Phys. Chem. B 103, 10965–10971.

Galkin, O., Vekilov, P.G., 2001. Nucleation of protein crystals: critical nuclei, phase behavior, and control pathways. J. Cryst. Growth 232, 63–76.

Gillespie, D.T., 1976. A general method for numerically simulating the stochastic time evolution of coupled chemical reactions. J. Comput. Phys. 22, 403–434.

Gillespie, D.T., 1977. Exact stochastic simulation of chemical reactions. J. Phys. Chem. 81, 2340–2361.

Gillespie, D.T., 1978. Monte Carlo simulation of random walks with residence time dependent transition probability rates. J. Comput. Phys. 28, 395–407.

Gillespie, D.T., 1992. A rigorous derivation of the chemical master equation. Physica A 188, 404–425.

Gillespie, D.T., 2001. Approximate accelerated stochastic simulation of chemically reacting systems. J. Chem. Phys. 115, 1716–1733.

Gillespie, D.T., 2007. Stochastic simulation of chemical kinetics. Annu. Rev. Phys. Chem. 58, 35–55.

Griffin, D.W., Mellichamp, D.A., Doherty, M.F., 2010. Reducing the mean particle size of API crystals by continuous manufacturing with product classification and recycle. Chem. Eng. Sci. 65, 5770–5780.

Hentschel, M.L., Page, N.W., 2006. Selection of descriptors for particle shape characterization. Part. Part. Syst. Charact. 20, 25–38.

Kalani, A., Christofides, P.D., 2002. Simulation, estimation and control of size distribution in aerosol processes with simultaneous reaction, nucleation, condensation and coagulation. Comp. Chem. Eng. 26, 1153–1169.

Ke, S.C., DeLucas, L.J., Harrison, J.G., 1998. Computer simulation of protein crystal growth using aggregates as the growth unit. J. Phys. D: Appl. Phys. 31, 1064–1070.

Kim, Y.C., Myerson, A.S., 1996. Diffusivity of protein in aqueous solutions. Korean J. Chem. Eng. 13, 288–293.

Kougoulos, E., Jones, A., Jennings, K., Wood-Kaczmar, M., 2005. Use of focused beam reflectance measurement (FBRM) and process video imaging (PVI) in a modified mixed suspension mixed product removal (MSMPR) cooling crystallizer. J. Cryst. Growth 273, 529–534.

Kurihara, K., Miyashita, S., Sazaki, G., Nakada, T., Suzuki, Y., Komatsu, H., 1996. Interferometric study on the crystal growth of tetragonal lysozyme crystal. J. Cryst. Growth 166, 904–908.

Kwon, J.S., Nayhouse, M., Christofides, P.D., Orkoulas, G., 2013a. Modeling and control of protein crystal shape and size in batch crystallization. AIChE J. 59, 2317–2327.

Kwon, J.S., Nayhouse, M., Christofides, P.D., Orkoulas, G. Protein crystal shape and size control in batch crystallization: comparing model predictive control with conventional operating policies. Ind. Eng. Chem. Res., in press. http://dx.doi.org/10.1021/ie400584g.

Kwon, J.S., Nayhouse, M., Christofides, P.D., Orkoulas, G., 2013b. Modeling and control of shape distribution of protein crystal aggregates. Chem. Eng. Sci. 104, 484–497.

Lawton, S., Steele, G., Shering, P., 2009. Continuous crystallization of pharmaceuticals using a continuous oscillatory baffled crystallizer. Org. Process Res. Develop. 13, 1357–1363.

Levenspiel, O., 1998. Chemical Reaction Engineering. Wiley Eastern.

Majumder, A., Nagy, Z., 2013. Fines removal in a continuous plug flow crystallizer by optimal spatial temperature profiles with controlled dissolution. AIChE J. 59, 4582–4594.

Müller, C., Liu, Y., Migge, A., Pietzsch, M., Ulrich, J., 2011. Recombinant L-asparaginase B and its crystallization—What is the nature of protein crystals? Chem. Eng. Technol. 34, 571–577.

Müller, C., Ulrich, J., 2011. A more clear insight of the lysozyme crystal composition. Cryst. Res. Technol. 46, 646–650.

Nanev, C.N., Tsekova, D., 2000. Heterogeneous nucleation of hen-egg-white lysozyme-molecular approach. Cryst. Res. Technol. 35, 189–195.

Nayhouse, M., Kwon, J.S., Christofides, P.D., Orkoulas, G., 2013. Crystal shape modeling and control in protein crystal growth. Chem. Eng. Sci. 87, 216–223.

Pourghahramani, P., Forssberg, E., 2005. Review of applied particle shape descriptors and produced particle shapes in grinding environments. Part 1: Particle shape descriptors. Miner. Process. Extr. Metall. Rev. 26, 145–166.

Pusey, M.L., Nadarajah, A., 2002. A model for tetragonal lysozyme crystal nucleation and growth. Cryst. Growth Des. 2, 475–483.

Rathinam, M., Petzold, L.R., Cao, Y., Gillespie, D.T., 2003. Stiffness in stochastic chemically reacting systems: the implicit tau-leaping method. J. Chem. Phys. 119, 12784–12794.

Reese, J.S., Raimondeau, S., Vlachos, D.G., 2001. Monte Carlo algorithms for complex surface reaction mechanisms: efficiency and accuracy. J. Comput. Phys. 173, 302–321.

Schmidt, L.D., 2005. The Engineering of Chemical Reactions. Oxford.

Shi, D., El-Farra, N.H., Li, M., Mhaskar, P., Christofides, P.D., 2006. Predictive control of particle size distribution in particulate processes. Chem. Eng. Sci. 61, 268–281.

Shi, D., Mhaskar, P., El-Farra, N.H., Christofides, P.D., 2005. Predictive control of crystal size distribution in protein crystallization. Nanotechnology 16, S562–S574.

Snyder, M.A., Chatterjee, A., Vlachos, D.G., 2005. Net-event kinetic Monte Carlo for overcoming stiffness in spatially homogeneous and distributed systems. Comput. Chem. Eng. 29, 701–712.

Suzuki, Y., Miyashita, S., Komatsu, H., Sato, K., Yagi, T., 1994. Crystal growth of hen egg white lysozyme under high pressure. Jpn. J. Appl. Phys. 33, 1568–1570.

Weber, M., Jones, M., Ulrich, J., 2008. Crystallization as a purification method for jack bean urease: on the suitability of poly(ethylene), Li_2SO_4 and NaCl as precipitants. Cryst. Growth Des. 8, 711–716.

Wong, S., Tatusko, A., Trout, B., Myerson, A., 2012. Development of continuous crystallization processes using a single stage MSMPR crystallizer with recycle. Cryst. Growth Des. 12, 5701–5707.